



1 **Short Communication: Aging of basalt volcanic systems and decreasing CO<sub>2</sub> consumption**  
2 **by weathering**

3 Janine Börker<sup>1</sup>, Jens Hartmann<sup>1</sup>, Gibran Romero-Mujalli<sup>1</sup>, Gaojun Li<sup>2</sup>

4 <sup>1</sup>Institute for Geology, CEN (Center for Earth System Research and Sustainability), Universität  
5 Hamburg, Bundesstraße 55, 20146 Hamburg, Germany. E-Mail: janine.boerker@uni-  
6 hamburg.de; geo@hates.de

7 <sup>2</sup>MOE Key Laboratory of Surficial Geochemistry, Department of Earth Sciences, Nanjing  
8 University, 163 Xianlindadao, Nanjing 210023, China

9 **Abstract**

10 Basalt weathering is one of many relevant processes balancing the global carbon cycle via land-  
11 ocean alkalinity fluxes. The CO<sub>2</sub> consumption by weathering can be calculated using alkalinity  
12 and is often scaled with runoff and/or temperature. Here it is tested if information on the surface  
13 age distribution of a volcanic system is a useful proxy for changes in alkalinity production with  
14 time.

15 A linear relationship between temperature normalized alkalinity fluxes and the Holocene area  
16 fraction of a volcanic field was identified, using information from 33 basalt volcanic fields, with  
17 an  $r^2=0.91$ . This relationship is interpreted as an aging function and suggests that fluxes from  
18 Holocene areas are ~10 times higher than those from old inactive volcanic fields. However, the  
19 cause for the decrease with time is probably a combination of effects, including a decrease in  
20 alkalinity production from surface near material in the critical zone as well as a decline in  
21 hydrothermal activity and magmatic CO<sub>2</sub> contribution.

22 A comparison with global models suggests, that global alkalinity fluxes considering Holocene  
23 active basalt areas are ~70% higher than the average from these models imply. The contribution  
24 of Holocene areas to the global basalt alkalinity fluxes is however only ~6%, because identified,  
25 mapped Holocene basalt areas cover only ~1% of the existing basalt areas. The large trap basalt  
26 proportion on the global basalt areas today reduces the relevance of the aging effect. However,  
27 the aging effect might be a relevant process during periods of globally, intensive volcanic  
28 activity, which remains to be tested.

29 **1. Introduction**

30 Basalt areas, despite its limited areal coverage, contribute significantly to the CO<sub>2</sub> sequestration  
31 by silicate rock weathering (Dessert et al., 2003; Gaillardet et al., 1999; Hartmann et al., 2009).  
32 The sensitivity of basalt weathering to climate change (Coogan and Dosso, 2015; Dessert et al.,  
33 2001; Dessert et al., 2003; Li et al., 2016) supports a negative weathering feedback in the carbon



34 cycle that maintains the habitability of the Earth's surface over geological time scales (Berner,  
35 1983; Li and Elderfield, 2013; Walker et al., 1981). Changes in volcanic weathering fluxes due  
36 to emplacement of large volcanic provinces or shifts in the geographic distribution of volcanic  
37 fields associated with continental drift may have contributed to climate change in the past  
38 (Goddéris et al., 2003; Kent and Muttoni, 2013; Schaller et al., 2012).

39 The role of basalt weathering in the carbon cycle and its feedback strength in the climate system  
40 depends, besides the release of geogenic nutrients, on the amount of associated CO<sub>2</sub> consumption  
41 and related alkalinity fluxes. The factors that modulate these fluxes are a subject to uncertainty.  
42 Previous studies suggest that basalt weathering contributes 25–35% to the global silicate CO<sub>2</sub>  
43 consumption by weathering (Dessert et al., 2003; Gaillardet et al., 1999; Hartmann et al., 2009).  
44 However, their estimations do not consider the potential aging of a weathering system. Young  
45 volcanic areas can show much higher weathering rates compared to older ones, as was shown for  
46 the Lesser Antilles, where a rapid decay of weathering rates within the first 0.5 Ma was observed  
47 (Rad et al., 2013). Such an aging effect of volcanic areas is difficult to parameterize for global  
48 basalt weathering fluxes, due to a lack of global compilations.

49 A practical approach to resolve this issue is to distinguish old and inactive volcanic fields (IVF)  
50 and active volcanic fields (AVF) (Li et al., 2016) and compare weathering fluxes with factors  
51 driving the weathering process, like land surface temperature or hydrological parameters. By  
52 compiling data from 37 basaltic fields globally, Li et al. (2016) showed that spatially explicit  
53 alkalinity fluxes (or CO<sub>2</sub> consumption rates) associated with basalt weathering correlate strongly  
54 with land surface temperature for IVFs, but not for AVFs. They suggested that previously  
55 observed correlations between weathering rates and runoff in global datasets originates partly  
56 from the coincidence of high weathering rates and high runoff of AVFs rather than a direct  
57 primary runoff control on the weathering rate. Many studied AVFs are located near the oceans  
58 and have an elevated topography, a combination, which can cause elevated runoff due to an  
59 orographic effect (Gaillardet et al., 2011). However, the here suggested aging effect on  
60 weathering rates from a volcanic system has not been evaluated.

61 The age distribution of the surface area of a whole volcanic system might be used as a first order  
62 proxy to study the variability of weathering fluxes of AVFs. However, the exact surface age of  
63 volcanic areas is rarely mapped in detail, but Holocene areas are often reported in geological  
64 maps. Here, basalt alkalinity fluxes are related to the calculated Holocene areal proportion of  
65 volcanic fields at the catchment scale. For this, the concept of weathering reactivity is  
66 introduced, which is the relative alkalinity flux of AVFs to the alkalinity flux estimated for IVFs  
67 by the function identified in Li et al. (2016). This reactivity  $R$  is compared with the relative age  
68 distribution of surface areas, using the fraction of the Holocene area on the total studied area.  
69 From this comparison a function for the decay of alkalinity fluxes with increasing proportion of  
70 older land surface area is derived and discussed.

71



## 72 **2. Methods**

73 The volcanic fields used to establish the relationship between weathering reactivity and  
74 Holocene coverage are predominantly described as basalt areas (Li et al., 2016). Based on the  
75 availability of detailed geological maps 33 volcanic provinces were selected, with 19 IVFs and  
76 14 AVFs. A detailed description is given in the supplementary information. The 14 AVFs are  
77 geographically widespread and diverse (Fig.1a). If the absolute age distribution of the volcanic  
78 rocks is available, the Holocene areas were mapped using the age range from 11.7 ka to present,  
79 according to the International Commission on Stratigraphy version 2017/02 (Cohen et al., 2013).  
80 If possible, coordinates of water sample locations were used to constrain catchment boundary to  
81 calculate the Holocene fraction for monitored areas. In some cases already existing alkalinity  
82 flux calculations were taken from Li et al. (2016). Detailed information on mapping and  
83 calculations for each system can be found in the supplementary information (SI).

The weathering reactivity (R) of each volcanic field is calculated by normalizing the observed alkalinity flux of the AVF ( $F_{observed}$ , in  $10^6 \text{ mol km}^{-2} \text{ a}^{-1}$ ) to that of the expected flux if the AVF would be an IVF ( $F_{expected}$ ) applying the previously identified weathering function for IVFs (Li et al., 2016):

$$84 \quad R = F_{observed}/F_{expected} \quad (\text{eq. 1})$$

85 where the expected alkalinity flux  $F_{expected}$  for IVFs is given by (Fig. 1b):

$$86 \quad F_{expected} (10^6 \text{ mol km}^{-2} \text{ a}^{-1}) = 0.2007 \times e^{(0.0692 \times T (^{\circ}\text{C}))} \quad (\text{eq. 2})$$

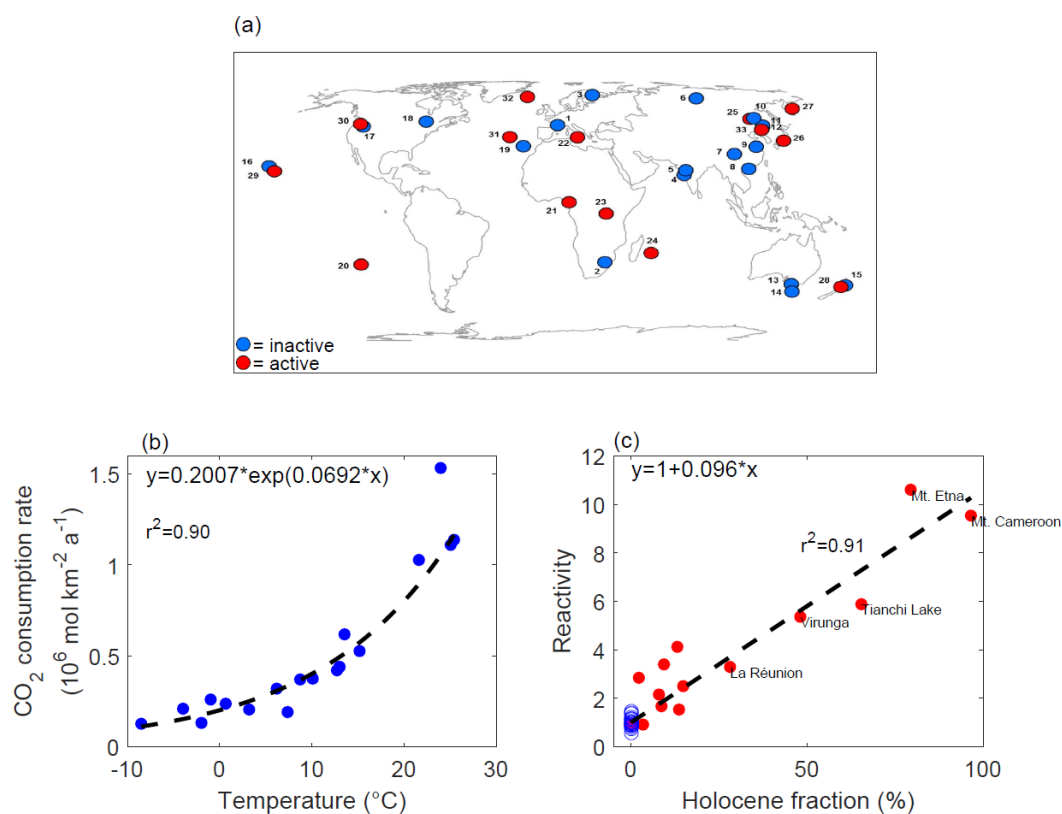


Figure 1. (a) The global map shows the locations of the Active Volcanic Fields (in red) and the Inactive Volcanic Fields (in blue) used in this study (1.Massif Central, 2.South Africa, 3.Karelia, 4.Coastal Deccan, 5.Interior Deccan, 6.Siberia Traps, 7.E'Mei, 8.Lei-Qiong, 9.Nanjing, 10.Xiaoxinganling, 11.Tumen River, 12.Mudan River, 13.SE Australia, 14.Tasmania, 15.North Island, NZ, 16.Kauai, Hawaii, 17.Columbia Plateau, 18.NE America, 19.Madeira Island, 20.Easter Island, 21.Mt.Cameroon, 22.Mt.Etna, 23.Virunga, 24.La Réunion, 25.Wudalianchi Lake, 26.Japan, 27.Kamchatka, 28.Taranaki, 29.Big Island, Hawaii, 30.High Cascades, 31.Sao Miguel, 32.Iceland, 33.Tianchi Lake). (b) The exponential relationship between alkalinity flux rates and the land surface temperature for IVFs (Li et al., 2016). (c) The relationship between the Holocene area fraction of a volcanic field and the weathering reactivity  $R$  ( $r^2=0.91$ ).

87 IVFs range around a reactivity  $R=1$  having a Holocene fraction of zero (Fig 1c). The reactivity  $R$   
 88 (eq. 1) of an AVF can be estimated by the Holocene area fraction as implied by the good linear  
 89 correlation identified in Fig. 1c. The virtual reactivity for Holocene areas can be estimated  
 90 rearranging eq. 1 and setting the area fraction to 100% :

$$91 \quad F_{\text{Holocene}} = R_{100\% \text{ Holocene}} * F_{\text{expected}} \quad (\text{eq. 3})$$



92 Global alkalinity fluxes from basalt areas are calculated using for older areas than of Holocene  
93 age equation 2 and for mapped Holocene areas equation 3. The model equations are calibrated  
94 for areas with a runoff  $> 74 \text{ mm a}^{-1}$  to avoid too high alkalinity fluxes from drier areas with high  
95 temperature (*e.g.*, the Sahara Desert), assuming that neglecting fluxes from areas with lower  
96 runoff are not biasing the comparison (Tab. S1, supplementary information). In this case an  
97 overestimation is avoided.

98 Results are compared with four previous global empirical alkalinity flux models (Bluth and  
99 Kump, 1994; Dessert et al., 2003; Goll et al., 2014; Suchet and Probst, 1995). Alkalinity fluxes  
100 were translated into  $\text{CO}_2$  consumption for allowing comparison with previous literature. For all  
101 models the same data input was used: a newly compiled global basalt map (mostly derived by the  
102 basalt lithological layer from the GLiM, but enhanced by mapped Holocene areas (SI; Hartmann  
103 and Moosdorf, 2012), additional regional geological maps reporting on basalt areas and the maps  
104 of the volcanic fields used in this study, for detailed information see supplementary information),  
105 temperature (Hijmans et al., 2005) and runoff (Fekete et al., 2002).

106

### 107 **3. Results and Discussion**

108 Studied IVFs are characterized by a Holocene volcanic surface area of 0% with weathering  
109 reactivity  $R$  ranging between 0.6 and 1.5 (Fig. 1c). In contrast, AVFs show a large range of  
110 Holocene coverage, from 0.2% (High Cascades) to 96.6% (Mount Cameroon), and weathering  
111 reactivity between 0.9 (Easter Island, High Cascades) and 10.6 (Mount Etna). The weathering  
112 reactivity correlates strongly with the percentage of Holocene area ( $r^2 = 0.91$ ; Fig. 1c),  
113 suggesting Holocene surface area distribution to be a good predictor for the enhanced alkalinity  
114 fluxes from a volcanic system:

$$115 \quad F_{\text{alkalinity}} = (1 + 0.096 \times H) \times 0.2007 \times e^{(0.0692 \times T)} [10^6 \text{ mol km}^{-2} \text{ a}^{-1}] \quad (\text{eq. 4})$$

116 where  $H$  is the Holocene fraction of a volcanic system in % and  $T$  is land surface temperature in  
117  $^{\circ}\text{C}$ .

118 The Holocene fraction is not interpreted as the physical cause for elevated alkalinity fluxes.  
119 Instead, magmatic  $\text{CO}_2$  contribution, geothermal-hydrothermal activity and the input of new  
120 volcanic material to the surface (properties and “freshness” of the surface area for reaction) are  
121 contributing to enhanced alkalinity fluxes.

122 The magmatic  $\text{CO}_2$  contributions to alkalinity fluxes in young volcanic systems may be large in  
123 general, but data are scarce to evaluate the global relevance for AVFs. For the Lesser Antilles a  
124 magmatic contribution of 23 to 40% to the  $\text{CO}_2$  consumed by weathering was identified (Rivé  
125 et al., 2013). High  $^{13}\text{C}$ -DIC values suggest that magmatic  $\text{CO}_2$  contributes significantly to the  
126 alkalinity fluxes from the Virunga system (Balagizi et al., 2015). The magmatic  $\text{CO}_2$  contribution



127 derived from volcanic calcite dissolution on Iceland was estimated to be about 10% of the  
 128 alkalinity fluxes for the studied area (Jacobson et al., 2015). In case of the Etna 7% of the CO<sub>2</sub>  
 129 emitted due to volcanic activity may be captured by weathering (Aiuppa et al., 2000). These  
 130 examples suggest that significant amounts of magmatic carbon may be transferred to the ocean  
 131 directly via intra-volcanic weathering from AVFs.

132 The calculated global basalt weathering alkalinity fluxes based on previous global models (Bluth  
 133 and Kump, 1994; Dessert et al., 2003; Goll et al., 2014; Suchet and Probst, 1995) give alkalinity  
 134 fluxes ranging between 0.7 to 1.6 × 10<sup>12</sup> mol a<sup>-1</sup>. These values are different to previously  
 135 published results based on the same models because a different geological map and climate data  
 136 are used in this study. The new calculation based on the temperature dependence of weathering  
 137 rate and the age dependence of weathering reactivity (eq. 4) results in higher global alkalinity  
 138 fluxes of 2 × 10<sup>12</sup> mol a<sup>-1</sup> and 3.4 × 10<sup>12</sup> mol a<sup>-1</sup> for regions with > 74mm a<sup>-1</sup> runoff, and for all  
 139 areas, respectively. The latter higher estimate is mainly due to the modeled contribution from dry  
 140 and hot regions and shows that it is relevant to apply the runoff cut off.

141 Using the new approach, considering the aging of a volcanic system, reveals that alkalinity  
 142 fluxes from Holocene areas contribute only 6% to the global basalt weathering alkalinity flux.  
 143 This is because identified mapped Holocene volcanic areas cover only ~1% of all basalt areas.

144 The Holocene area is probably underestimated due to information gaps in the reported age  
 145 information of the global map. The strong dependence of weathering reactivity on relative age of  
 146 the surface of a considered volcanic system suggests that it is relevant to know the global spatial  
 147 age distribution of volcanic areas in more detail. Therefore, a new global review of the age  
 148 distribution of basalt areas would be needed, which is beyond the scope of this study.

149

*Table 1: Summary of CO<sub>2</sub> consumption rates for global basaltic areas applying different models and the new parameterization. For simplicity it was assumed that alkalinity fluxes equal CO<sub>2</sub> consumption.*

150

		Global CO <sub>2</sub> consumption rate (10 <sup>9</sup> mol/a) for limited area in comparison (only areas with > 74mm/a runoff)	Global CO <sub>2</sub> consumption rate (10 <sup>9</sup> mol/a)
Dessert et al. 2003	runoff, temperature	1567	1573
Amiotte-Suchet & Probst, 1995	runoff	838	843
Bluth & Kump, 1994	runoff	739	754
Goll et al., 2014	runoff, temperature	1471	1477
New equation	temperature	1992	3431

151



152 The applied time stamp of the Holocene boundary suggests that the aging of the “weathering  
153 motor” of a basaltic volcanic area, including internal weathering, with declining volcanic activity  
154 is rather rapid. This implies that peaks in global volcanic activity have probably a short but  
155 intensive effect on the CO<sub>2</sub> consumption. A pronounced effect on the global carbon cycle by  
156 shifting the global reactivity of volcanic areas may only be relevant for geological periods with  
157 significantly elevated production of new volcanic areas, accompanied by geothermal-  
158 hydrothermal activity and capture of magmatic CO<sub>2</sub> before its escape to the atmosphere.

159 Results may have relevance for the carbon cycle and climate studies considering the  
160 displacement of large igneous provinces like the CAMP (Schaller et al., 2012) or the Deccan  
161 traps (Caldeira, 1990) with production of large basaltic areas within a short time. However, the  
162 biological contribution to CO<sub>2</sub> drawdown, via fertilization effects, *e.g.* P- or Si-release due to  
163 weathering and elevated CO<sub>2</sub> in the atmosphere must also be taken into account.

164 Looking deeper into Earth’s history: variations in the solid Earth CO<sub>2</sub> degassing rate or changes  
165 in environmental conditions affecting the weathering intensity (Hartmann et al., 2017; Teitler et  
166 al., 2014) may have caused different reactivity patterns in dependence of surface age, if  
167 compared to the ones identified for the recent conditions.

168 In conclusion, a simple approach to detect an aging effect, using surface age as a proxy for  
169 several combined processes, was chosen due to availability of data. Nevertheless, the combined  
170 effect on elevated weathering reactivity due to magmatic CO<sub>2</sub> contribution, hydrothermal  
171 activity, production of fresh surface area for reaction, and hydrological factors of young volcanic  
172 systems remains to be disentangled, for single volcanic systems, as well as for the emplacement  
173 of larger, trap-style basalt areas.

#### 174 **Acknowledgements:**

175 Funding for this work has been provided by German Research Foundation (DFG) through the  
176 Cluster of Excellence CLISAP2 (DFG Exec177, Universität Hamburg), and BMBF-project  
177 PALMOD (Ref 01LP1506C) through the German Federal Ministry of Education and Research  
178 (BMBF) as Research for Sustainability initiative (FONA).

#### 179 **6. References**

- 180 Aiuppa, A. et al., 2000. Mobility and fluxes of major, minor and trace metals during basalt weathering  
181 and groundwater transport at Mt. Etna volcano (Sicily). *Geochimica et Cosmochimica Acta*,  
182 64(11): 1827-1841.
- 183 Balagizi, C.M. et al., 2015. River geochemistry, chemical weathering, and atmospheric CO<sub>2</sub> consumption  
184 rates in the Virunga Volcanic Province (East Africa). *Geochemistry, Geophysics, Geosystems*,  
185 16(8): 2637-2660.
- 186 Berner, R.A., Lasaga, A.C., Garrels, R.M., 1983. The carbonate-silicate geochemical cycle and its effect on  
187 atmospheric carbon dioxide over the past 100 million years. *Am J Sci*, 283: 641-683.





- 188 Bluth, G.J., Kump, L.R., 1994. Lithologic and climatologic controls of river chemistry. *Geochimica et*  
189 *Cosmochimica Acta*, 58(10): 2341-2359.
- 190 Caldeira, K., Rampino, M.R., 1990. Carbon dioxide emissions from Deccan volcanism and a K/T boundary  
191 greenhouse effect. *Geophysical Research Letters*, 17(9): 1299-1302.
- 192 Cohen, K., Finney, S., Gibbard, P., Fan, J.-X., 2013. The ICS international chronostratigraphic chart.  
193 *Episodes*, 36(3): 199-204.
- 194 Coogan, L.A., Dosso, S.E., 2015. Alteration of ocean crust provides a strong temperature dependent  
195 feedback on the geological carbon cycle and is a primary driver of the Sr-isotopic composition of  
196 seawater. *Earth and Planetary Science Letters*, 415: 38-46.
- 197 Dessert, C. et al., 2001. Erosion of Deccan Traps determined by river geochemistry: impact on the global  
198 climate and the 87Sr/86Sr ratio of seawater. *Earth and Planetary Science Letters*, 188(3-4): 459-  
199 474.
- 200 Dessert, C., Dupré, B., Gaillardet, J., François, L.M., Allègre, C.J., 2003. Basalt weathering laws and the  
201 impact of basalt weathering on the global carbon cycle. *Chemical Geology*, 202(3-4): 257-273.
- 202 Fekete, B.M., Vörösmarty, C.J., Grabs, W., 2002. High - resolution fields of global runoff combining  
203 observed river discharge and simulated water balances. *Global Biogeochemical Cycles*, 16(3).
- 204 Gaillardet, J., Dupré, B., Louvat, P., Allègre, C.J., 1999. Global silicate weathering and CO<sub>2</sub> consumption  
205 rates deduced from the chemistry of large rivers. *Chemical Geology*, 159(1-4): 3-30.
- 206 Gaillardet, J. et al., 2011. Orography-driven chemical denudation in the Lesser Antilles: Evidence for a  
207 new feed-back mechanism stabilizing atmospheric CO<sub>2</sub>. *American journal of science*, 311(10):  
208 851-894.
- 209 Goddérís, Y. et al., 2003. The Sturtian 'snowball' glaciation: fire and ice. *Earth and Planetary Science*  
210 *Letters*, 211(1-2): 1-12.
- 211 Goll, D.S., Moosdorf, N., Hartmann, J., Brovkin, V., 2014. Climate-driven changes in chemical weathering  
212 and associated phosphorus release since 1850: Implications for the land carbon balance.  
213 *Geophysical Research Letters*, 41(10): 3553-3558.
- 214 Hartmann, J., Jansen, N., Dürr, H.H., Kempe, S., Köhler, P., 2009. Global CO<sub>2</sub>-consumption by chemical  
215 weathering: What is the contribution of highly active weathering regions?
- 216 Hartmann, J., Li, G., West, A.J., 2017. Running out of gas: Zircon 18O-Hf-U/Pb evidence for Snowball  
217 Earth preconditioned by low degassing. *Geochemical Perspectives Letters*, 4: 41-46.
- 218 Hartmann, J., Moosdorf, N., 2012. The new global lithological map database GLiM: A representation of  
219 rock properties at the Earth surface. *Geochemistry, Geophysics, Geosystems*, 13(12): n/a-n/a.
- 220 Hijmans, R.J., Cameron, S.E., Parra, J.L., Jones, P.G., Jarvis, A., 2005. Very high resolution interpolated  
221 climate surfaces for global land areas. *International journal of climatology*, 25(15): 1965-1978.
- 222 Jacobson, A.D., Grace Andrews, M., Lehn, G.O., Holmden, C., 2015. Silicate versus carbonate weathering  
223 in Iceland: New insights from Ca isotopes. *Earth and Planetary Science Letters*, 416: 132-142.
- 224 Kent, D.V., Muttoni, G., 2013. Modulation of Late Cretaceous and Cenozoic climate by variable  
225 drawdown of atmospheric  $\text{CO}_2$  from weathering of basaltic provinces on  
226 continents drifting through the equatorial humid belt. *Clim. Past*, 9(2): 525-546.
- 227 Li, G., Elderfield, H., 2013. Evolution of carbon cycle over the past 100 million years. *Geochimica et*  
228 *Cosmochimica Acta*, 103: 11-25.
- 229 Li, G. et al., 2016. Temperature dependence of basalt weathering. *Earth and Planetary Science Letters*,  
230 443: 59-69.
- 231 Rad, S., Rivé, K., Vittecoq, B., Cerdan, O., Allègre, C.J., 2013. Chemical weathering and erosion rates in  
232 the Lesser Antilles: An overview in Guadeloupe, Martinique and Dominica. *Journal of South*  
233 *American Earth Sciences*, 45: 331-344.





- 234 Rivé, K., Gaillardet, J., Agrinier, P., Rad, S., 2013. Carbon isotopes in the rivers from the Lesser Antilles:  
235 origin of the carbonic acid consumed by weathering reactions in the Lesser Antilles. *Earth*  
236 *Surface Processes and Landforms*, 38(9): 1020-1035.
- 237 Schaller, M.F., Wright, J.D., Kent, D.V., Olsen, P.E., 2012. Rapid emplacement of the Central Atlantic  
238 Magmatic Province as a net sink for CO<sub>2</sub>. *Earth and Planetary Science Letters*, 323–324: 27-39.
- 239 Suchet, P.A., Probst, J.L., 1995. A global model for present-day atmospheric/soil CO<sub>2</sub> consumption by  
240 chemical erosion of continental rocks (GEM-CO<sub>2</sub>). *Tellus B*, 47(1-2): 273-280.
- 241 Teitler, Y., Le Hir, G., Fluteau, F., Philippot, P., Donnadiou, Y., 2014. Investigating the Paleoproterozoic  
242 glaciations with 3-D climate modeling. *Earth and Planetary Science Letters*, 395: 71-80.
- 243 Walker, J.C.G., Hays, P.B., Kasting, J.F., 1981. A negative feedback mechanism for the long-term  
244 stabilization of Earth's surface temperature. *Journal of Geophysical Research: Oceans*, 86(C10):  
245 9776-9782.
- 246